Modeling Interferogram Stacks

Fabio Rocca

***Abstract*—Synthetic aperture radar interferometry is limited by temporal and geometrical decorrelation. Permanent scatterers (PSs) are helpful to overcome these problems, but their density in agricultural and out-of-town areas is not always sufficient. The forthcoming availability of satellite platforms with thinner orbital tubes and shorter revisit times will enhance the use of interferogram stacks, which are usable for distributed and progressively decorrelating targets, like those found in agricultural areas. To estimate the possibilities of the interferogram stack technique, a Markovian model for the temporal decorrelation is considered. ERS-1 data measured in C-band over Rome with a three-day repeat cycle are used to identify the parameters for this model, namely, the decorrelation time (estimated as 40 days) and the short-term coherence (estimated as 0.6). In the hypothesis of small deviations from a model of the motion, the optimal weights to be used to combine a sequence of interferograms taken at intervals that are shorter than the decorrelation time are calculated in the cases of progressive and sinusoidal ground motion. The dispersion of the optimal estimate of the motion is then determined. This model is extended to frequencies other than C-band. These evaluations are compared with the known results obtained for PSs. As an example, the case of a time interval between the takes of $T = 12$ days is considered. With N consecutive images, interferogram stack results are equivalent to PSs if the pixel count in the window used to smooth the interferograms grows with N^2.**

***Index Terms*—Differential interferometric SAR (DInSAR), interferometric SAR (InSAR), synthetic aperture radar (SAR).**

I. Introduction

SINCE 1991, synthetic aperture radar (SAR) data that are systematically taken every 35 days have been made available by the European Space Agency (ESA) European Remote Sensing (ERS-1) satellite. The successive ESA satellites ERS-2 and ENVISAT and the availability of the Canadian satellite Radarsat with its 24-day revisit time allowed more data to be considered for multipass SAR interferometry. The reader is referred to [1], [6], and [16] for a general view of SAR interferometry. In this paper, I will try to identify the advantages that will be obtained using shorter revisit time satellites, like GMES Sentinel 1 [17], that should be orbited in the next decade. With the current satellites, the usefulness or, rather, the need [3] for long-term stable scatterers [the so-called permanent or persistent scatterers (PSs)] has long been established to 1) reduce the effects of a) temporal decorrelation and b) geometric decorrelation [8] due to the wide orbital tubes and 2) abate the influence of the atmospheric phase screen (APS). However, as soon as new SAR satellites with shorter revisiting times, wider radio-frequency bandwidth, and thinner orbital tubes will be available, distributed scatterer interferometry will also be an interesting tool to estimate slow terrain subsidence, tectonic effects, and slow landslides. Subsidence estimates based either on PSs or interferogram stacks will thus be available. Here, I evaluate the dispersion of the ground motion estimate using both techniques at different frequencies. For that, I model the scatterer's temporal decorrelation law. I use a Brownian model of the scatterer change, i.e., I suppose that each scatterer within the cell will randomly walk along the line of sight. The parameters for this model are derived from the three-day revisit interval data, which were obtained by ERS-1 in the ice phase in 1993. The outcome is an exponentially decreasing correlation and the decorrelation time constant in C-band in lightly vegetated areas is estimated to be approximately 40 days; this time constant can be easily extrapolated to other frequencies. Then, any interferogram stack technique becomes a weighted stack of the interferograms at different spans. The optimal weights to combine the interferograms are then determined, taking also into account their mutual correlation. For a given revisit time, the weights depend on the carrier frequency, and shorter spans are to be preferred at shorter wavelengths. Notice that the subsidence estimate could be directly obtained from the N images, rather than from the $N(N-1)/2$ interferograms, apparently in a simpler way. However, the estimation becomes more difficult, and here, I propose the longer but easier way. For an analysis of the alternative technique, i.e., operating on the phases rather than on the interferograms, please see [18].

After a brief summary of differential SAR (DInSAR) interferometry, I assess the accuracy of the ground motion estimate with conventional DInSAR and with the PS technique at different frequencies. I assume a simplified SAR acquisition, where the Earth is flat, and the sensor orbits are straight and parallel. This assumption is well justified on a local scale, i.e., for assessing performances in terms of the accuracy of the ground motion estimate for progressive motion. Finally, I evaluate the quality of the estimate of periodical motion. I conclude that in C-band, with a 12-day revisit interval, about 100 pixels, exponentially decorrelating with an average decorrelation time of 40 days, should yield an estimate of progressive motion that is as good as that yielded by a PS.

II. Interferogram Stacks

Many targets in a SAR image are not coherent over long temporal intervals; nevertheless, they can be exploited for motion estimation using "conventional" DInSAR techniques. Despite the widely developed literature on differential interferometry, starting from the very first InSAR references

Manuscript received December 14, 2006; revised March 25, 2007. This work was supported in part by the European Space Agency under Contract 19142/05/NL/CB.

The author is with the Dipartimento di Elettronica ed Informazione, Politecnico di Milano, 20133 Milano, Italy (e-mail: rocca@elet.polimi.it).

Digital Object Identifier 10.1109/TGRS.2007.902286

(see [7] and [9]), there has been a substantial lack of estimates of the decorrelation of distributed targets, as well as optimal techniques to provide an estimate of the motion field, after the paper by Zebker and Villasenor [21]. Most approaches can be generally defined as "interferogram stacks," and new and appealing methodologies [12] that could be classified in this category appear. However, there is no clear and formal assessment of the actual processing required. Even in the most recent papers (see, e.g., [5]), the motion estimate is, indeed, a somewhat heuristic exploitation of a set of interferograms that were taken with the shortest temporal baselines possible, where the choice of the interferograms to be combined is based on a data-driven recipe that tries to get the best results, accounting for target decorrelation and atmospheric artifacts. This is also due to the fact that, up to now, no satellite has been fully dedicated to interferometry; hence, no complete sequences of interferometric images abound [2]. Further, the multiplication of modes offered by the current satellites adds another complication, i.e., even if the same area is imaged in subsequent passes, the imaging will not be necessarily carried out in the same mode. Furthermore, the wide orbital tubes used are beneficial to PS interferometry but hinder distributed scatterer coherence. In the future, narrower orbital tubes are to be expected; thus, this becomes a further motivation to study interferogram stacks.

I establish a model for target decorrelation and provide a statistically consistent estimator to be mainly used for the assessment of the ground motion accuracy. I first focus on uniform subsidence. The optimal estimation of the subsidence rate in millimeter per year v is quite complicated because of the presence of target decorrelation, additive noise (clutter more than thermal), and multiplicative noise due to the APS, i.e., the delay introduced by water vapor and ionospheric plasma [10]. In particular, the latter contributions make the probability density function of the observations non-Gaussian and difficult to express in a closed form. The presence of phase aliasing further jeopardizes the data statistics and the achievement of a consistent solution. I approach the problem in a very simple way: by approximating the APS as an additive noise, as it is reasonable for the expected phase dispersion on the order of 1 rad. However, unlike PS interferometry, DInSAR surveys can have large decorrelation and a small signal-to-noise ratio (SNR) (the reflection can be weak), and APS cannot be really approximated as additive noise (its standard deviation may be, at times, larger than 1 rad). In that case, an exact maximum-likelihood estimate can be derived by a more refined statistical analysis. This has been done and will be fully reported soon [18].

III. Modeling the Decorrelation

A. Exponential Model: Brownian Motion

I suppose that the time decorrelation mechanism is primarily due to the motion of the scatterers in the resolution cell. I model this motion as a Brownian motion, or the sum of many successive independent and equally distributed motions so that the normal approximation holds (see [21]). It is possible to substitute the variable describing the motion (in the line of sight) with the variable describing the (unwrapped) phase because of the linear relation between the two. The complex reflectivity $\xi(t)$ becomes $\xi(t+nT)$ after nT. The only difference between the two is in the phase; thus, I can actually express the second as a function of the first, i.e.,

$$\xi(t+nT) = \xi(t)\exp(-j\varphi)$$

where φ is itself a real random variable that is normally distributed and independent from $\xi(t)$, with variance σ_φ^2. Assuming the motion to be Brownian implies that the phase variance σ_φ^2 linearly increases with the time interval, i.e., $\sigma_\varphi^2 = \sigma^2 nT$. The decorrelation law is

$$\gamma(nT) = E\left[\xi(t)\xi^*(t+nT)\right] = e^{-\frac{nT}{\tau}} = \rho^n \tag{3.1}$$

where $\tau = 2/\sigma^2$. For instance, for a Brownian motion in the look direction with a standard deviation in a day of $\sigma_{\mathrm{Bd}}/\sqrt{\mathrm{day}}$, with, e.g., $\sigma_{\mathrm{Bd}} = 1$ mm, the phase deviation would be

$$\sigma = \sigma_{\mathrm{Bd}}\frac{4\pi}{\lambda}\ \mathrm{rad}\cdot\mathrm{day}^{-\frac{1}{2}}. \tag{3.2}$$

Hence, we have the following equations:

$$\rho = e^{-T/\tau} = e^{-1/M} \quad M = \frac{\tau}{T} = \frac{2}{T\sigma_{\mathrm{Bd}}^2}\left(\frac{\lambda}{4\pi}\right)^2 \tag{3.3}$$

which correspond to a time constant $\tau = 40$ days in C-band. This was for a single scatterer. If the resolution cell contains many scatterers so that the observed reflectivity is the sum of elemental contributions, then the coherence shows the same exponential decay with time, provided that each element is affected by an independent Brownian motion.

B. Exponential Model: Markov

This alternative model makes the assumption that the elemental scatterers in the resolution cell suddenly change their reflectivity, passing from complete coherence to zero. Once a start time is set $(t_0 = 0)$, the scatterers are divided in two classes: those that have experienced at least one change and those that have not. There are two populations: the unchanged n_{UN} and the changed ones $n_{\mathrm{CH}}(t)$, with $n_{\mathrm{UN}}(t) + n_{\mathrm{CH}}(t) = n_{\mathrm{TOT}} = \mathrm{const}$. At any given time, provided that the scatterers have similar amplitude statistics, the coherence is proportional to the expected number of unchanged scatterers, i.e.,

$$\gamma(t) = \frac{E\left[n_{\mathrm{UN}}(t)\right]}{n_{\mathrm{TOT}}}. \tag{3.4}$$

Suppose the change rate is constant and the process is without memory other than the state. Then, the differential variation of the unchanged population is proportional to the current unchanged population, i.e.,

$$\frac{dE\left[n_{\mathrm{UN}}(t)\right]}{dt} = -\frac{E\left[n_{\mathrm{UN}}(t)\right]}{\tau} \rightarrow E\left[n_{\mathrm{UN}}(t)\right] = n_{\mathrm{TOT}} \times e^{-t/\tau} \tag{3.5}$$

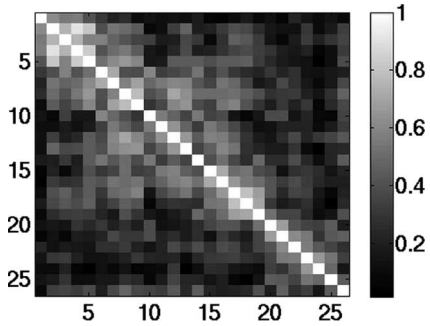

Fig. 1. Covariance matrices of Rome data, ordered with the acquisition date and showing an approximately exponential decay.

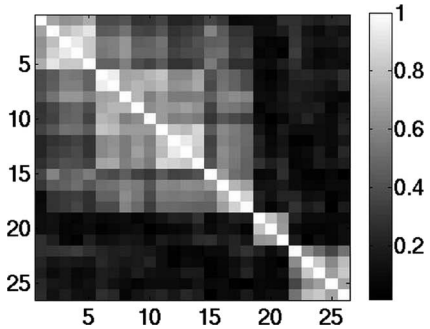

Fig. 2. Covariance matrices of Rome data, ordered with the acquisition date and showing a Markovian behavior.

which is equivalent to the Brownian motion model. A more complex model could consider different populations $p_1, p_2, \ldots, p_N$ $(\sum_n p_n = 1)$ that are characterized by different time constants. In this case, the time evolution is

$$\gamma(nT) = \sum_n p_n e^{-nT/\tau_n}. \tag{3.6}$$

In the case of only two populations with very different τ (e.g., τ_2 is very small compared to the acquisition time scale), the coherence can be approximated with

$$\gamma(nT) = p_1 e^{-nT/\tau_1}. \tag{3.7}$$

The term p_1 in (3.7) can range from 1 to 0 and represents the fraction of the scatterers that did not suffer from a "quick decorrelation" mechanism. The impact of decorrelation is the same as that of thermal noise, i.e., a multiplication by

$$\gamma_{\mathrm{SNR}} = \frac{1}{1 + \mathrm{SNR}^{-1}}. \tag{3.8}$$

Then, I account for all the multiplicative terms with a single constant γ_0, and eventually, the model simply writes as follows:

$$\gamma(nT) = \gamma_0 e^{-nT/\tau} = \gamma_0 \rho^n. \tag{3.9}$$

C. Identification of Model Parameters

The parameters of the exponential models can be identified using estimates of coherence. In the data sets that have been exploited, the sampled estimate [14] has been applied to the interferogram after removing the topographic contribution by means of a digital elevation model. The estimation window has been made sufficiently large to minimize the bias of the estimate [19]. The result is a series of matrices, each of them representing the correlation properties in a particular place in the scene (actually, the estimation window). Two examples are provided in Figs. 1 and 2. The images are arranged by the acquisition date (26 images are available), and each element in the matrix represents the coherence of a pair. The principal diagonal is always unitary because every image is perfectly coherent with itself. In Fig. 2, it is easy to recognize three separate moments in the scatterer's "life." To obtain the coherence as a function of time separation, I take all the pairs in the data set, spanning the same interval (for instance, all the pairs with a temporal baseline of 15 days), and I average their coherence to make the estimates more robust, i.e.,

$$\hat{\gamma}(nT) = \frac{\sum_{t(k_2)-t(k_1)=nT} \hat{\gamma}(k_1, k_2)}{\sum_{t(k_2)-t(k_1)=nT} 1} \tag{3.10}$$

where $t(k)$ is the time of the kth acquisition. This is the input to the next stage, which is the identification of the model.

The parameters of the model that can best justify the observations can then be found. The identification process consists of trying many combinations of the parameters and choosing the best one according to some figure of merit Q. In this case, the L_1 norm is minimized, i.e.,

$$Q(\gamma_0, \tau) = \sum_{nT} \left| \hat{\gamma}(nT) - \gamma_0 e^{-nT/\tau} \right|. \tag{3.11}$$

The sum is extended to all nTs for which an estimate $\hat{\gamma}(nT)$ is available. The output of the identification step is the triple $\hat{\gamma}_0$, $\hat{\tau}$, and $Q(\hat{\gamma}_0, \hat{\tau})$ for each processed window.

IV. Validation With Real Data

The results discussed here are based on scenes from an ERS-1 ice-phase data set (Track 22, Frame 2763) that was acquired over central Italy from the end of December 1993 to April 1994 (26 scenes). During this acquisition phase, the revisit time interval was three days, whereas all the other orbital parameters remained basically unchanged. The images were focused and oversampled by a factor of 2 (range only) and coregistered on the master's common grid (the image was taken on March 5, 1994). Then, a portion of the entire scene was selected (20 $\times$ 15 km, range $\times$ azimuth). It is near the Fiumicino (Rome, Italy) airport and shows the last part of the Tevere River course. This C-band data set peculiarity stays with the reduced revisit time, which is just three days. This characteristic is very important in studying the decorrelation dynamics in the time span of a few weeks: a task that is much harder with the more common 35-day data set. Although the maximum baseline span is about 800 m, I chose to work with a reduced set of 17 images in the range of $\pm$250 m. This measure is an attempt to reduce the impact of geometric decorrelation. At the same time, I applied spectral shift filtering in the range band common

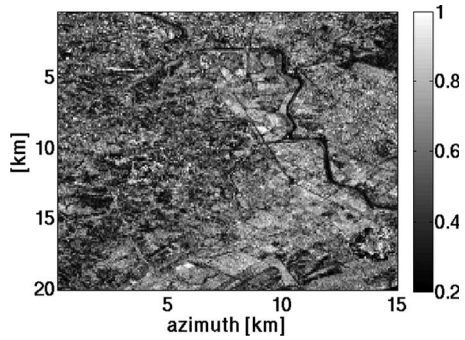

Fig. 3. Map of the short-term coherence γ_0.

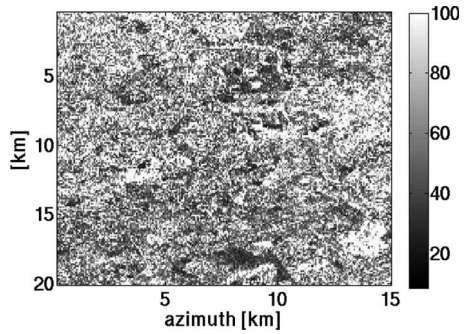

Fig. 4. Map of the time constant τ.

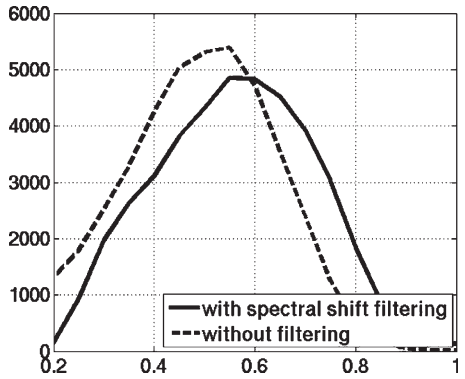

Fig. 5. Histogram of the short-term coherence γ_0, with and without spectral shift filtering.

to *all* images [8]. Approximately half the original bandwidth was retained by this step, as one is limited by the worst case (500 m).

A. Decorrelation Dynamics

Estimates have been made by spatial averaging on a 12×12 pixel window (range oversampled $2:1$), and no overlap between any two windows was allowed to make every measure independent. Figs. 3 and 4 show the maps for the short-term coherence γ_0 and for the estimated time constant τ. The histograms of the short-term coherence and the time constant τ, with and without spectral shift filtering, are shown in Figs. 5 and 6.

The peak in the histogram is at about 40–50 days. As expected, the coherence is increased if the common band-filtered images are used, because a source of decorrelation is eliminated. The histograms clearly indicate an increase in coherence with filtering. The reason for not having any point with $\hat{\gamma}_0$ lower than 0.2 can be explained by the estimate bias discussed earlier in this paper. In fact, even for large time spans over totally decorrelated areas, it would be usual to find coherence measures higher than 0.15. Forcing an exponential model to explain such observations brings us to the conclusion that the "starting coherence" $\hat{\gamma}_0$ must be greater than or equal to such a value.

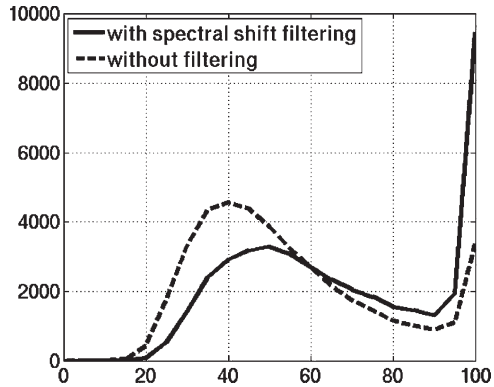

Fig. 6. Histogram of the time constant τ, with and without spectral shift filtering.

B. Joint Distribution of the Estimates

The joint distribution of $\hat{\tau}$ and $\hat{\gamma}_0$ seemed to be separable, which makes the two parameters independent. To further analyze the problem, I applied a singular value decomposition on the matrix that approximates the joint probability density. If it were a dyad, i.e., with a prevailing eigenvalue, the matrix would be separable. In our case, the first eigenvalue is about ten times the second.

V. Linear Estimates of Ground Motion

A. Covariance Matrix of the Interferograms

In this section, I will deal with the approximate estimation of the progressive interferometric phase, namely, the subsidence velocity correspondent to an additional phase shift ϕ that is identical from one pass to the next. We have

$$\phi = \frac{4\pi v T}{\lambda} \tag{5.1}$$

where T is the interval between the takes, and λ is the wavelength. The interferogram is obtained by cross multiplying two images at times $k_1 T$ and $k_2 T$ and then averaging over L pixels. The removal of the scatterer's phases is obtained by multiplying one image times the conjugate of the other. In this derivation, I suppose that the baseline is systematically zero, and thus, I will not consider geometrical decorrelation. This impacts on the covariance of the decorrelation noise as well, which is now dependent only on temporal decorrelation. As the subsidence-induced phase shifts could create geometrical decorrelation, if changing with the range, I have assumed to have uniform subsidence in all the pixels to be considered. The value of L is determined by hypothesizing that all pixels stay within the correlation radius of the APS, e.g.,

within 800 m, and are therefore subject not only to the same subsidence mentioned before, but also to the same atmospheric phase. The interferogram value is given by

$$F_{k_1k_2} = \frac{1}{L}\sum_{h=1}^{L} z_{h,k_1} z^*_{h,k_2}$$

where z is the received signal considered as the sum of the temporally decorrelating signal γx plus noise n, i.e.,

$$z = \gamma x + n. \tag{5.2}$$

The expected value of the interferogram is

$$E[F_{k_1k_2}] = E\left[z_{h,k_1} z^*_{h,k_2}\right] = \gamma_{k_1k_2}\sigma_x^2 + \sigma_n^2\delta(k_1 - k_2)$$

where $\gamma_{k_1k_2}$, which is the temporal component of the coherence, can be expressed on the basis of the exponential decay (3.9) as

$$\gamma_{k_1k_2} = \rho^{|k_1-k_2|} \tag{5.3}$$

and ρ is real and smaller than 1. In short, I will call *span* the temporal baseline of an interferogram, i.e., the time interval $(|k_1 - k_2|T)$ between the two takes, whereas *lag* will be the delay between the time centers of two interferograms either with the same span or with different spans. Further, σ_x^2 is the variance of the complex value of the noiseless received signal x_{h,k_i} that is supposed to be constant with h, k_i. The actual coherence will be lower than $\gamma_{k_1k_2}$ due to the additive noise n (e.g., the instantaneous decorrelation term). By using the exponential Markov model, the temporal component of the coherence exponentially decreases with the span. By indicating with ρ the coherence at span T and considering the phase shifts due both to the progressive subsidence and to the APS and, therefore, adding to the subsidence phase shifts a_{k_1} and a_{k_2} due to the APS in the two takes, I get

$$\gamma_{k_1k_2} = \rho^{|k_1-k_2|} e^{j\left[(k_2-k_1)\phi + a_{k_1} - a_{k_2}\right]}.$$

For small phase shifts, I can linearize with respect to the APS and subsidence terms, i.e.,

$$\gamma_{k_1k_2} \sim \rho^{|k_1-k_2|}\left[1 + j\left((k_2 - k_1)\phi + a_{k_1} - a_{k_2}\right)\right]. \tag{5.4}$$

It is correct to contend that even if the subsidence could be low, the APS will not be. In effect, we expect σ_a, i.e., the rms value of the APS to be on the order of 1 rad [10]. The dispersion of the two-way additional travel path due to local random variations of the refractivity of the atmosphere is

$$\sigma_r \sim 10\ [\text{mm}] \tag{5.5}$$

and then

$$E\left[a_k^2\right] = \sigma_a^2 = \left(\frac{2\pi\sigma_r}{\lambda}\right)^2. \tag{5.6}$$

Further, we are referring to a single position in the image, and we can expect that we will be able to predict, at least partially, the value of the APS in that position from the neighboring points. This, in turn, even after a few iterations, would lead to much smaller values for the residual APS and, therefore, to the feasibility of this linearization.

Notice that there is a further approximation here: the phase shifts due to subsidence and APS are attached to the coherence, i.e., to the mean of the correlation between the two images and not to the actual value of the sampled average. In other words, I am neglecting the second-order biasing effect due to the phase shift of the decorrelation noise. This effect would be irrelevant in the case of equal variance of the real and imaginary parts of the decorrelation noise, but as the variance of the real part is always larger than that of the imaginary one and much more so if the coherence is high, as we will see in the sequel, this approximation may have some impact.

The interferogram covariance for any given atmospheric and subsidence phase shift, by using the Gaussianity of the data and the Gaussian moment factoring theorem, is

$$\begin{aligned}\text{Cov}[F_{k_1k_2}F_{k_3k_4}] =& \frac{E\left[\sum_{h,k=1}^{L} z_{h,k_1} z^*_{h,k_2} z^*_{k,k_3} z_{k,k_4}\right]}{L^2} \\ &- E[F_{k_1k_2}]E\left[F^*_{k_3k_4}\right] \\ =& \frac{E[F_{k_1k_3}]E\left[F^*_{k_2k_4}\right]}{L}.\end{aligned} \tag{5.7}$$

I introduced here the set of all the interferograms, i.e., $N(N-1)/2$ complex numbers per pixel, instead of the original N images. There is, apparently, an unjustified explosion of the number of degrees of freedom: for N independent numbers (the images), we get $N(N-1)/2$ only partially correlated interferograms (obviously, never independent). This is easy to check, as for $\gamma = 0$, the covariance matrix of the interferograms is diagonal, as it will be better seen in the following. Therefore, it is clear that it would be much better to directly estimate the parameter ϕ from the original image phases themselves, rather than by combining interferograms. However, the phases are non-Gaussian, the optimal estimate (the conditional mean) is a nonlinear function of the data, and the Cramér–Rao bound becomes more difficult to interpret. This problem is solved in this paper [18].

B. Optimal Linear Estimates

Exploiting the small phase approximation (5.4) and the consequent linearization, I will now consider only the imaginary parts of the interferograms $\mathcal{I}_{k_1k_2}$ that were averaged over L pixels, which were supposed to have the same APS. This averaging process will allow us to hypothesize that the averaged interferogram is a Gaussian variate, for the central limit theorem, to be described with its mean plus an additional noise $n'(k_1, k_2)$ to be combined with the effects of the supposedly small phase shifts induced by APS and subsidence. After the linearization in (5.4), the imaginary part of the interferogram, considering the additive noise to the signal and temporal decorrelation, is

$$\begin{aligned}\text{Im}(F_{k_1k_2}) =& \mathcal{I}_{k_1k_2} \sim \rho^{|k_1-k_2|}\sigma_x^2\left[(k_2 - k_1)\phi + a_{k_1} - a_{k_2}\right] \\ &+ n'(k_1, k_2) \\ n'(k_1, k_2) =& \text{Im}\left[F_{k_1k_2} - E[F_{k_1k_2}]\right].\end{aligned} \tag{5.8}$$

We indicate with $n'(k_1, k_2)$ the random variate—real and zero mean—corresponding to the imaginary part of the interferogram that is not dependent on APS or subsidence. Notice that the variances of the real parts and the imaginary parts of the interferograms are different. For an intuitive confirmation of that, let us consider the case of no temporal decorrelation, no subsidence, or no APS, i.e., a flat interferogram with coherence that is equal to one. Although the phase and, therefore, the imaginary part of the interferogram is zero, the interferogram is a nonzero-mean random real variate, as it is the square modulus of a Gaussian variate. Hence, with good coherence, we expect, in general, many changes along the real parts of the interferograms and much smaller changes along their imaginary parts.

Now, I construct a vector $\underline{\mathbf{F}}$ with the imaginary parts of all the $N(N-1)/2$ interferograms, which were arranged using the first image in the interferograms first, then the second, etc., without repetitions, as follows:

$$\underline{\mathbf{F}}^T = [\mathcal{I}_{12}\, \mathcal{I}_{13}\, \ldots\, \mathcal{I}_{1N};\quad \mathcal{I}_{23}\, \mathcal{I}_{24}\, \ldots\, \mathcal{I}_{2N};\quad \ldots\, \mathcal{I}_{N-1,N}]. \tag{5.9}$$

Rather than indicate the entries of this vector with one index, for simplicity, I use the two indexes of the images that contributed to the interferogram. $\underline{\mathbf{F}}$ is the sum of the three random vectors $\phi\underline{\mathbf{M}}$, $(a_{k_1} - a_{k_2})\underline{\mathbf{A}}$, and $\underline{\mathbf{N}}$, i.e.,

$$\underline{\mathbf{F}} = \phi\underline{\mathbf{M}} + (a_{k_1} - a_{k_2})\underline{\mathbf{A}} + \underline{\mathbf{N}} = \phi\underline{\mathbf{M}} + \underline{\mathbf{B}}$$

which is sorted like (5.9) and represents the following.

1) $\phi\underline{\mathbf{M}}$ is the progressive phase shifts, e.g., due to subsidence, with entries $\phi(k_1 - k_2)\rho^{|k_1-k_2|}\sigma_z^2$.
2) $(a_{k_1} - a_{k_2})\underline{\mathbf{A}}$ is the APS with entries $(a_{k_1} - a_{k_2})\rho^{|k_1-k_2|}\sigma_z^2$ (for an easier check of the formulas).
3) $\underline{\mathbf{N}}$ represents the contributions to the imaginary part of the interferograms due to instantaneous and progressive temporal decorrelation. The covariance matrix relative to $\underline{\mathbf{F}}$ is the sum of three covariance matrices, which are related to the three random vectors that have just been introduced. The matrix due to the random subsidence rate ϕ is a dyad, which is expressed by

$$E[\phi^2\underline{\mathbf{M}}\underline{\mathbf{M}}^*] \to \sigma_\phi^2\sigma_x^4\rho^{|k_1-k_2|+|k_3-k_4|}(k_1 - k_2)(k_3 - k_4)$$

and that due to the APS is

$$E\left[(a_{k_1}-a_{k_2})\underline{\mathbf{A}}(a_{k_3}-a_{k_4})\underline{\mathbf{A}}^*\right] = \sigma_a^2\sigma_x^4\rho^{|k_1-k_2|+|k_3-k_4|}\begin{pmatrix}+\delta(k_1-k_2)+\delta(k_3-k_4)\\ -\delta(k_2-k_4)-\delta(k_1-k_3)\end{pmatrix}. \tag{5.10}$$

It is possible to check that the entries of the correlation matrix of the imaginary parts of the interferograms, without the additional phase shifts due to APS or ground motion, are

$$E[\underline{\mathbf{N}}\underline{\mathbf{N}}^*] \to \frac{\begin{matrix}\sigma_x^4(\gamma_{k_1k_2}\gamma_{k_3k_4} - \gamma_{k_1k_4}\gamma_{k_2k_3}) + \\ \sigma_x^2\sigma_n^2\begin{bmatrix}+\delta(k_1-k_3)\gamma_{k_2k_4} + \delta(k_1-k_4)\gamma_{k_2k_3}\\ -\delta(k_2-k_4)\gamma_{k_1k_3} - \delta(k_2-k_3)\gamma_{k_1k_4}\end{bmatrix}\\ +\sigma_n^4\left(\delta(k_1-k_3)\delta(k_2-k_4) - \delta(k_1-k_4)\delta(k_2-k_3)\right)\end{matrix}}{2L} \tag{5.11}$$

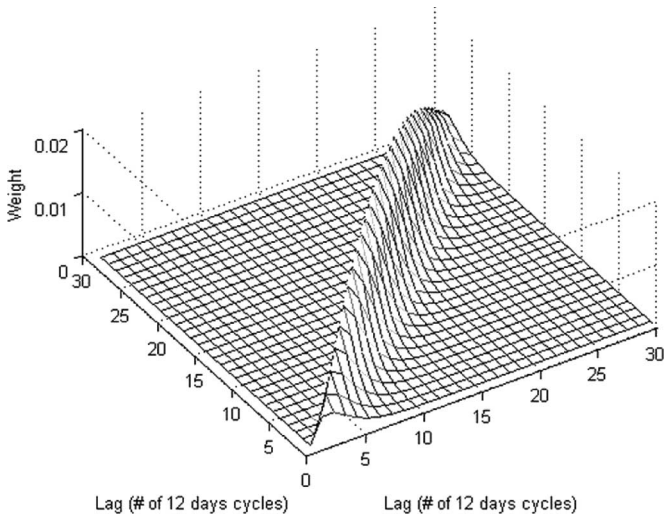

Fig. 7. Moduli of the interferogram weights as a function of time lags k_1 and k_2, $k_2 > k_1$: $\rho = 0.74$, $\gamma_0 = 0.6$, and $N = 30$. Approximately five lags are used.

For the real parts, the negative signs of the contributions become positive, and thus, the sum is consistent with (5.7). The dispersion of the phases σ_ϕ^2 of an interferogram can be expressed as the ratio between the dispersion of the imaginary part over the squared mean as follows:

$$k_1 = k_3 \quad k_2 = k_4 = k_1 + 1 \quad E[F] = \rho\sigma_x^2 \tag{5.12}$$

$$\sigma_\phi^2 = \frac{1-\rho^2}{2L\rho^2} \tag{5.13}$$

which is consistent with [21] if σ_n^2 is considered part of the decorrelation mechanism. As mentioned before, for $\gamma = 0$, the covariance matrix $E[\underline{\mathbf{F}}\underline{\mathbf{F}}^*]$ is diagonal, notwithstanding the dimensionality being much higher than the original data set. Notice that for $N = 30$ images, I have $N(N-1)/2 = 435$ interferograms, and this is the size of the covariance matrices. The optimal estimate of ϕ is a linear combination of the interferograms weighted with the weight vector $\underline{\mathbf{P}}^*$, i.e.,

$$\widehat{\phi} = \underline{\mathbf{P}}^*\underline{\mathbf{F}} = \underline{\mathbf{P}}^*(\phi\underline{\mathbf{M}} + \underline{\mathbf{B}}).$$

The weights can be computed by imposing incorrelation between the data (the interferograms) and the error, i.e.,

$$E\left[\underline{\mathbf{F}}(\underline{\mathbf{F}}^*\underline{\mathbf{P}} - \phi)\right] = \underline{\mathbf{0}} \tag{5.14}$$

By whitening the noise and imposing an unbiased estimate (i.e., the limit of the previous one for $\sigma_\phi^2 \to \infty$), following [20], we are led to the following expression of the weight vector:

$$\underline{\mathbf{P}} = \frac{\underline{\mathbf{M}}^*\underline{\mathbf{Q}}^{-1}}{\underline{\mathbf{M}}^*\underline{\mathbf{Q}}^{-1}\underline{\mathbf{M}}} \qquad \underline{\mathbf{Q}} = E[\underline{\mathbf{B}}\underline{\mathbf{B}}^*]$$

which is represented in Fig. 7. The weight vector is represented as a function of the two indexes corresponding to the two takes; for this figure, the total number of takes is 30, and thus, the matrix is 30×30. However, the matrix is zero on and below the main diagonal, as the autointerferograms are irrelevant (points on the main diagonal), and each interferogram is considered

only once. In the case of no instantaneous decorrelation, and no APS, only the interferograms at span 1 (those on the first subdiagonal) are used. The instantaneous decorrelation smoothes this matrix. The APS induces smaller weights for the interferograms at the beginning and the end of the takes, as the chaining of the interferograms (and, thus, the compensation of the APS) is broken at both ends of the takes. Finally, the error variance is

$$\lim_{\sigma_\phi^2 \to \infty} E\left[(\phi - \widehat{\phi})^2\right] = \frac{1}{\underline{\mathbf{M}}^* \underline{\mathbf{Q}}^{-1} \underline{\mathbf{M}}}.$$

These equations will be revisited in Section V-C, in the cross-spectral domain, to simplify them and make them more directly understandable. The final results will then be summarized in Fig. 10.

Finally, before going further into the discussion, one has to remember that the sample covariance matrix of the pixels, namely, the matrix of the cross correlations of the interferograms, as it is a sum of L dyads, has size $N \times N$ and at most rank L, whereas the sample covariance matrix of the interferograms has size $N(N-1)/2 \times N(N-1)/2$ and rank 1. Therefore, one has to reduce the dimensionality of the problem to achieve some statistical estimate [13]. Indeed, one can always introduce spatiotemporal averaging procedures to augment the rank of the matrices, but all averaging processes, unless data dependent and, therefore, nonlinear, hinder the identification of PSs. Therefore, skillful averaging techniques should be found, where an optimal use is made of the temporal and spatial dimensions (like, e.g., averaging over seasons or target similarities).

C. Cross Spectra of Interferogram Sequences

I can simplify the problem by considering sequences of interferograms $F_m^{(p)}$ with a given span $2p$; the index m corresponds to the center time of the interferogram. The previously given formulas simplify, in a symmetrical presentation, to

$$m = \frac{k_1 + k_2}{2} \quad n = \frac{k_3 + k_4}{2}$$
$$p = \frac{k_2 - k_1}{2} \quad q = \frac{k_4 - k_3}{2}, \qquad p, q > 0 \tag{5.15}$$

where the indexes n and q correspond to the center time and span $2q$ of the second interferogram, respectively.

By indicating further the lag between two interferograms with l and with h and k the values

$$l = n - m \quad h = \frac{p - q}{2} \quad k = \frac{p + q}{2}$$

we have

$$k_1 = m - p \quad k_1 - k_4 = l - 2k \quad \cdots$$

and we gain the following simple relation:

$$\frac{L}{\sigma_x^4} \mathrm{Cov}\left[F_m^{(q)} F_{m+l}^{(p)}\right] = \rho^{2\max(|l|,|h|)} + \frac{2\delta(l)}{\mathrm{SNR}} + \frac{\delta(l)\delta(h)}{\mathrm{SNR}^2}. \tag{5.16}$$

Therefore, the complex covariance of two interferograms depends only on their lag l and on the span difference. The covariances of the real and imaginary parts depend also on the span sum. To find the estimator, rather than studying the cross correlations of the interferograms in the span and lag domains, I look at their cross spectra, particularly at their low-frequency components that will be amplified by the interferogram stacks. As interferogram stacking is the low-pass filtering of the interferogram sequence, I move to the spectral domain, and I indicate with ψ the Fourier conjugate of the interferogram center times m and n. In this way, the analysis will be simplified as the interferograms center times m and n and the lags $l = n - m$ disappear and instead of the initial four indexes (namely, the current ones k_1, k_2, k_3, and k_4 or the symmetrized ones, i.e., lags and spans m, n, p, and q), we have just the two spans, i.e., p and q, and some behavior with the frequency ψ. As always, we suppose that $\rho^N \sim 0$, i.e., that the sequence is much longer than the decorrelation time. APS and temporal decorrelation effects decouple, allowing a general simplification.

The correlation between the zero-frequency components of the cross spectra of the imaginary parts of the interferograms that have spans p and q is indicated with $\mathcal{N}_{\mathrm{dec},pq}(\psi = 0)$. This component of the cross spectrum is the sum of all the lags of the autocorrelation function (or mutual correlation function) of the imaginary parts between the interferograms at spans p and q. The sum is finite due to the previous hypothesis on the finite decorrelation time. The elements of the cross-spectral matrix of the imaginary parts of the interferograms at zero frequency depend on the difference and the sum of their spans (the lags are averaged out) and are

$$\begin{aligned}\frac{2L\mathcal{N}_{\mathrm{dec},pq}(\psi = 0)}{\sigma_x^4} &= \rho^{2|p-q|}\left(2|p-q| + \frac{1+\rho^2}{1-\rho^2}\right) \\ &\quad - \rho^{2|p+q|}\left(2|p+q| + \frac{1+\rho^2}{1-\rho^2}\right) \\ &\quad + \frac{2\left(\rho^{2|p-q|} - \rho^{2|p+q|}\right)}{\mathrm{SNR}} + \frac{\delta(p-q)}{\mathrm{SNR}^2}.\end{aligned} \tag{5.17}$$

The cross spectra of the atmospheric perturbations at very low frequencies (at zero frequency, they are zero) are calculated as follows. The atmospheric noise contribution correlation comes from terms like

$$\sigma_z^4 \sigma_a^2 \rho^{2p+2q} \left[(a_{m-p} - a_{m+p})(a_{n-q} - a_{n+q})\right].$$

The cross correlations of the atmospheric contributions between interferograms with spans p and q, termed $r_{\mathrm{atm},pq}(l)$, are in the center time domain, and for lag l, we have

$$\begin{aligned}r_{\mathrm{atm},pq}(l) = \sigma_x^4 \sigma_a^2 \rho^{2(p+q)} &[\delta(l-2h) \\ &+ \delta(l+2h) - \delta(l-2k) + \delta(l+2k)].\end{aligned}$$

By Fourier transforming in ψ, we derive

$$\begin{aligned}\mathcal{N}_{\mathrm{atm},pq}(\psi) &= \rho^{4k}\sigma_x^4\sigma_a^2(e^{-j2\psi h} + e^{j2\psi h} - e^{-j2\psi k} - e^{-j2\psi k}) \\ &= 2\rho^{4k}\sigma_x^4\sigma_a^2(\cos 2\psi h - \cos 2\psi k)\end{aligned}$$

and approximating for low frequencies, we have

$$\begin{aligned}\mathcal{N}_{\mathrm{atm},pq}(\psi) &= 4\rho^{4k}\sigma_x^4\sigma_a^2\psi^2(k^2-h^2)\\ &= 4pq\rho^{2(p+q)}\sigma_x^4\sigma_a^2\psi^2, \qquad \psi \ll 1.\end{aligned}$$

Hence, the cross-spectral matrix of the APS contribution at low frequencies is a dyad that increases with ψ^2. Finally, the signal components are expressed by

$$\mathcal{N}_{\mathrm{sig},pq}(\psi) = 4pq\rho^{2(p+q)}\sigma_\phi^2\sigma_x^4\delta(\psi)$$

i.e., the same dyad but with a delta-like frequency behavior instead of ψ^2 for the atmosphere. The estimate of the interferometric phase ϕ in the presence of this colored noise can be carried by averaging over N samples of the interferograms, i.e., windowing the spectrum. I approximate this windowing with an ideal filter in the band as follows:

$$\left|\frac{\psi N}{2}\right| < \frac{\pi}{2} \rightarrow |\psi| < \frac{\pi}{N}.$$

If the decorrelation time is much shorter than the integration time NT, then in the band of the filter, the cross spectrum of the decorrelation can be considered as a constant. In conclusion, the entries of the cross-spectral matrices of the different sources of noise that are integrated in this band are indicated with $\overline{\mathcal{N}}_{\mathrm{dec},pq}$, $\overline{\mathcal{N}}_{\mathrm{atm},pq}$ and are given by

$$\begin{aligned}\frac{2LN}{\pi\sigma_x^4}\overline{\mathcal{N}}_{\mathrm{dec},pq} &= \rho^{2|p-q|}\left(2|p-q| + \frac{1+\rho^2}{1-\rho^2}\right)\\ &\quad - \rho^{2|p+q|}\left(2|p+q| + \frac{1+\rho^2}{1-\rho^2}\right)\\ &\quad + \frac{2\left(\rho^{2|p-q|} - \rho^{2(p+q)}\right)}{\mathrm{SNR}} + \frac{\delta(p-q)}{\mathrm{SNR}^2}\\ \frac{N}{\pi}\frac{\overline{\mathcal{N}}_{\mathrm{atm},pq}}{\sigma_x^4} &\sim \frac{4}{3}\left(\frac{\pi}{N}\right)^2\sigma_a^2 pq\rho^{2(p+q)}. \qquad (5.18)\end{aligned}$$

The signal vector $\underline{s}$ has the following components:

$$\phi s_p = 2\rho^{2p}p\phi\sigma_x^2 \quad \underline{s}^T = \sigma_x^2[\rho, 2\rho^2, 3\rho^3, \ldots].$$

The interferogram cross-spectral vector I_p (in slanted characters; its version in the time domain was in calligraphic characters) is now the vector of the interferogram stacks at span p, and rather than $N(N-1)/2$, it has a much smaller size N_{cs}, which corresponds to the maximum span to be used for the estimation, e.g., 5. Thus, we have

$$\begin{aligned}1 \le p \le N_{\mathrm{cs}} < N\\ I_p = [I_1, I_2, \ldots I_{N_{\mathrm{cs}}}]\\ E[\underline{II}^*] = \overline{\underline{\mathcal{N}}} = \overline{\underline{\mathcal{N}}}_{\mathrm{dec}} + \overline{\underline{\mathcal{N}}}_{\mathrm{atm}} + \sigma_\phi^2\underline{ss}^*. \qquad (5.19)\end{aligned}$$

There is a misconception here that should be identified. If we have N images, we have $N-1$ samples of the 1 span interferogram sequence, but only one sample of the $N-1$ span interferogram sequence. To have the cross spectra of the windowed sequences, we need an equal number of samples for the sequences of interferograms at all spans $p \le N_{\mathrm{cs}}$, and this is what we do not have. However, as $N_{\mathrm{cs}} < N$ because the decorrelation time for distributed scatterers is, in general, much shorter than the observation time, this error in the cross-spectral analysis is not very significant. Anyway, the previous analysis in the time domain does not have this problem. Proceeding as before, the unbiased optimal estimate of the subsidence rate leads to the following expression of the error:

$$E\left[(\phi - \widehat{\phi})^2\right] = \frac{1}{\underline{s}^*(\overline{\underline{\mathcal{N}}}_{\mathrm{dec}} + \overline{\underline{\mathcal{N}}}_{\mathrm{atm}})^{-1}\underline{s}}.$$

Then, exploiting the fact that

$$\overline{\underline{\mathcal{N}}}_{\mathrm{atm}} = \frac{\sigma_a^2}{3}\left(\frac{\pi}{N}\right)^3\underline{ss}^* \qquad (5.20)$$

and using the matrix inversion lemma, I have

$$E\left[(\phi - \widehat{\phi})^2\right] = \frac{1}{3}\left(\frac{\pi}{N}\right)^3\sigma_a^2 + \frac{\pi}{2LN}\frac{1}{\underline{s}^*\overline{\underline{\mathcal{N}}}_{\mathrm{dec}}^{-1}\underline{s}} \qquad (5.21)$$

where the entries of the matrix $\overline{\underline{\mathcal{N}}}_{\mathrm{dec}}$ are $\overline{\underline{\mathcal{N}}}_{\mathrm{dec},pq}$ for the spans p and q and are reported in (5.17). The optimal weights depend only on ρ and SNR, which is consistent with (5.21). The weights $\underline{\beta}$ of the interferogram stacks at different spans are shown in Fig. 8 in the case when $\rho = \exp(-12/40)$ and SNR $= 1.5$. In this case, even interferograms at significant spans could profitably be used, thus increasing the size N_{cs} of the matrix $\underline{\mathcal{N}}_{\mathrm{dec}}$. Notice that, due to our approximations, the effect of the atmosphere is not the correct one ($\pi^3/3 = 10.3 < 12$). Luckily, however, in this approximation, the variance of the estimate is the sum of the variances due to atmosphere and decorrelation: one decreases as $1/N^3$ and the other as $1/N$. The behavior is PS like if the first component prevails.

It is possible to notice from (5.21) that the distributed scatterers act as a PS, i.e., the APS is the main cause for dispersion

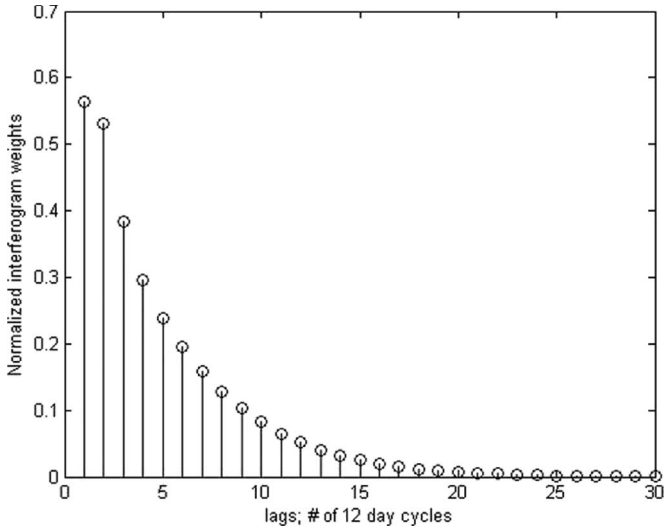

Fig. 8. Interferogram stack weights as a function of the lag: $\rho = 0.74$, SNR $= 1.5$, and $N = 30$.

of the subsidence rate estimate if the number of looks is greater than

$$L_{\rm PS} = \frac{3}{2\pi^2}\frac{N^2}{\sigma_a^2}\frac{1}{\underline{s}^*\underline{\mathcal{N}}_{\rm dec}^{-1}\underline{s}}. \tag{5.22}$$

If M is the number of revisits during the decorrelation time constant, i.e., from (3.3), we have

$$M = \frac{\tau}{T} = -\frac{1}{\log\rho} \tag{5.23}$$

it so happens that it results approximately to

$$\underline{s}^*\underline{\mathcal{N}}_{\rm dec}^{-1}\underline{s} \sim 0.2M + \gamma_0 - 1 = 0.2M - \frac{1}{1+\text{SNR}}. \tag{5.24}$$

Then, the still rather complex formula (5.22) can be approximated with the following very simple one, even frequency independent, as it will be seen in the last section. To avoid (in)significant figures, then, if T is the repeat time in weeks, we have

$$L_{\rm PS} \sim 0.75\frac{N^2}{M\sigma_a^2} = 0.1N^2T \text{ [in weeks]}. \tag{5.25}$$

1) Discussion: The result in (5.25) is reasonable in that the dispersion of the estimate of the subsidence rate decreases with N^3 in the case of a PS. In the case of L distributed scatterers decorrelating in M revisits, we combine sequences of N interferograms at M spans, on L pixels, and thus, the dispersion may well decrease with MNL. Then, to make the two behaviors equivalent, one needs L increasing with $N^2/M\sigma_a^2$. In our case, $M\sigma_a^2 \sim 3$. This model, very crude and overestimating $L_{\rm PS}$ as the atmospheric contribution is very small, still captures the interesting behavior of $L_{\rm PS}$ versus frequency, as will be seen in Section VII. In fact, as long as the product $M\sigma_a^2$ is slowly varying with λ, the frequency will minimally create an impact on $L_{\rm PS}$. Further, it is easy to check that with a high SNR, one span suffices, and the others become redundant, as the unique source of noise is decorrelation. This corresponds to, e.g., the observation that the inverse of a Toeplitz exponential matrix is tridiagonal, or that with first-order Markov processes, the memory to use for estimations is as short as possible. With a lower SNR, more spans are useful. Anyway, with the expected spatial resolution of 5 × 20 m, we expect well more than 50 independent APS measurements per square kilometer, which is not bad at all. This would allow a good estimate of the APS, its reduction, and, therefore, the justification of the assumptions made, entering the PS regime and yielding a further reduction of the dispersion of the velocity estimate.

D. Unbiased Estimates of Sinusoidal Motion Processes

The linear approximation that I have used allows to extend the evaluation of the error to any motion, and it is not necessarily relative to a constant subsidence rate. It is enough to use, as vector to be estimated, a sinusoidal change with time, at any given pulsation ψ_h. In this case, the vector $\phi\underline{\mathbf{M}}$ becomes

$$\phi\underline{\mathbf{M}} = \phi_h(e^{jk_1\psi_h} - e^{jk_2\psi_h}) \quad \psi_h = \frac{2\pi}{N}h; \qquad h = 1,\ldots,N.$$

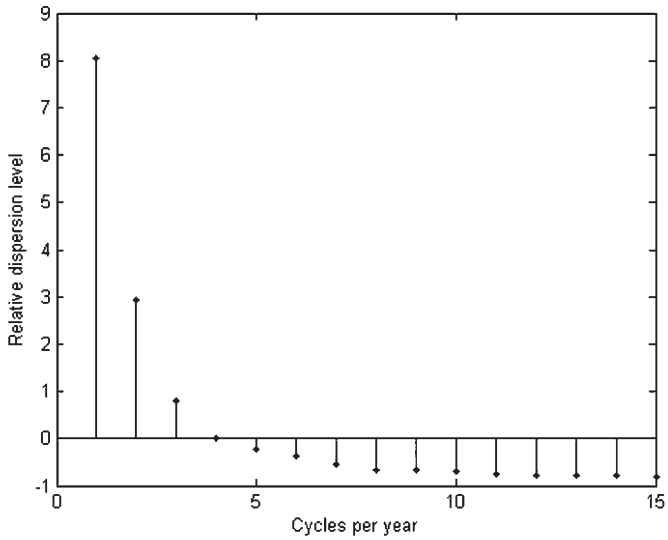

Fig. 9. Noise level as a function of the temporal frequency, which is normalized to the seasonal variation.

The unbiased minimum variance estimate of the component of the motion ϕ_h at pulsation ψ_h is found with the same methodology as before, i.e., following the unbiased estimator that Capon uses for his spectral analysis [20]. In Fig. 9, I show the error as a function of the frequency, which is normalized to a seasonal variation, in the case of 30 images per year and 50 looks. The behavior ramps up between 0.5 and 0.25 cycles/year. For zero frequency, the dispersion is unlimited: a constant phase is irretrievable. As the noise due to temporal change is correlated and, thus, low-pass, faster motions are less affected.

VI. PS Interferometry

In PSs, the target is assumed to be a stable point scatterer. The sole meaningful information is then its complex amplitude in the nominal target location. The contribution due to the subsidence for the nth image is

$$z_n = |A|\exp j\psi\exp\left(j\frac{4\pi}{\lambda}vnT\right) + w_n \tag{6.1}$$

where A is the amplitude of the scatterer, w_n is the noise contribution that mainly accounts for thermal noise, clutter, and (small) target decorrelation, and ψ is the intercept, i.e., the offset in the subsidence linear law that is combined with the phase of the scatterer. In PS interferometry, I assume that the amplitude of the target's return is much larger than the noise, so that I may approximate the phase of each single observation as

$$\angle z_n = \psi + \frac{4\pi}{\lambda}vnT + \phi_n^c \tag{6.2}$$

where ϕ_n^c is a zero-mean normal noise that accounts for clutter, thermal noise, and target long-term coherence. Its variance is

half the ratio of the peak power of the target in the SLC SAR image to the noise power, i.e.,

$$\sigma_c^2 = \frac{\sigma_{wn}^2}{2A^2} = \frac{\mathrm{SNR}_s^{-1}}{2}.$$

If I assume that phases due to APS are zero-mean normally distributed, I get the following model:

$$\angle z_n = \psi + \frac{4\pi}{\lambda} vnT + \phi_n^c + \phi_n^a + \phi_n^t \tag{6.3}$$

$$= \psi + \frac{4\pi}{\lambda} vnT + \phi_n^w \tag{6.4}$$

where ϕ_n^a is the APS noise. In (6.4), I have added all the noise contributions in a single one, i.e., ϕ_n^w, which is still zero-mean normal, and its variance is the superposition of all the contributions, which is given as follows:

$$\sigma_w^2 = \sigma_c^2 + \sigma_a^2 + \sigma_t^2.$$

Model (6.4) is the one assumed for estimating the subsidence rate v. Notice that the intercept ψ is a nuisance parameter in the sense that I do not explicitly require its estimate. Model (6.4) can be solved by linear regression. As a simple example, if I assume $N = 30$ data takes, i.e., a one-year span, assuming a GMES-Sentinel 1 (GS1) $d = 12$ days repeat interval, I get the following subsidence rate error:

$$\sigma_{v_p} \simeq \frac{\lambda}{4\pi} \frac{365}{d} \sigma_\phi \sqrt{\frac{12}{N^3 - N}} \simeq 3.6 \text{ mm/year} \tag{6.5}$$

$$\sigma_\phi = \sqrt{\sigma_a^2 + \sigma_{\mathrm{SNR}}^2} = \sqrt{\left(\frac{2\pi\sigma_r}{\lambda}\right)^2 + \frac{1}{2 \cdot \mathrm{SNR}}} \tag{6.6}$$

where σ_ϕ is the phase dispersion of the PS and is due to the contribution σ_a^2 of the APS, as $\sigma_r = 10$ mm is the two-way travel path dispersion due to atmospheric effects (5.5) and (5.6) and to the phase dispersion due to SNR

$$\sigma_{\mathrm{SNR}}^2 \simeq \frac{1}{2 \cdot \mathrm{SNR}}. \tag{6.7}$$

This last contribution is the cause of the higher dispersion at longer carrier wavelengths (e.g., P-band). I have assumed for the PS that usually have higher radar cross section that SNR $\rightarrow$ 10 dB. Expression (6.3) is the fundamental one to be used for assessing the accuracy of the subsidence rate estimation in PS interferometry. Notice that this result accounts for an isolated PS, and I am not considering the possibility of abating the atmospheric noise by averaging its estimate on neighboring PSs. Further, the problem of phase unwrapping has not been approached. However, it is very unlikely to occur if the standard deviation of the error is quite lower than π: in any case, ignoring unwrapping errors will give a lower bound on the rate estimate.

VII. Extension of the Model to Different Frequencies

One advantage of the model that has been considered is the possibility of its extension to different carrier wavelengths λ.

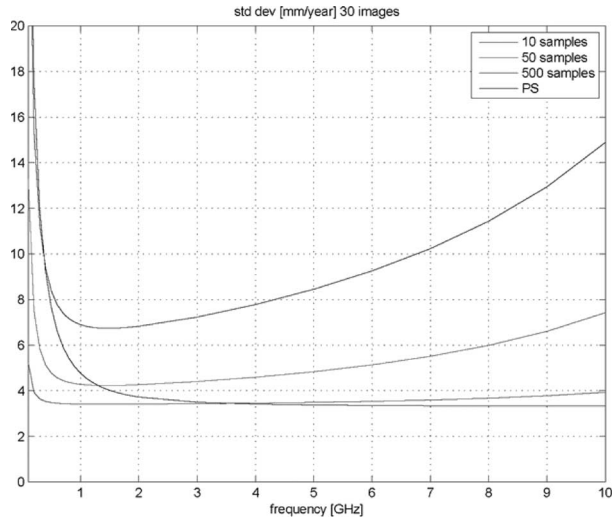

Fig. 10. Dispersion of the estimate of the subsidence rate is shown as a function of frequency for different values of the number of looks ($L = 10, 50, 500$ and $N = 30$) and for a PS.

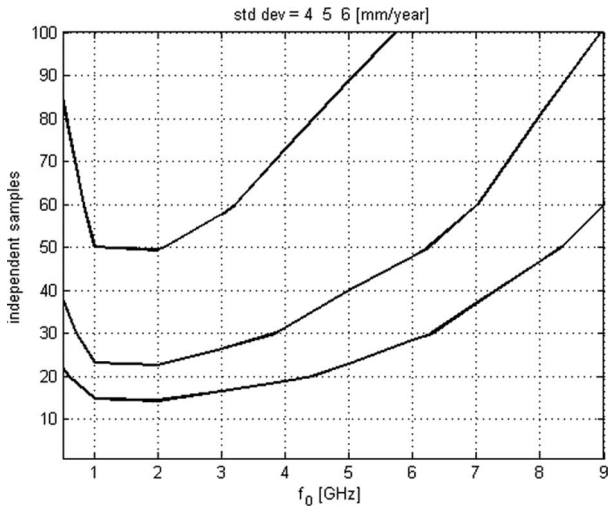

Fig. 11. Number of pixels equivalent to a PS as a function of frequency for various velocity dispersions (4, 5, and 6 mm/year; 12 days repeat).

The decorrelation at span 1 and the rms atmospheric phase shift, according to (3.3), become

$$\rho = \exp\left(-\frac{1}{M}\right) \qquad M = \frac{\tau}{T} = \frac{2}{\sigma_{\mathrm{Bd}}^2 T}\left(\frac{\lambda}{4\pi}\right)^2 \tag{7.1}$$

$$\sigma_a^2 = \left(\frac{2\pi\sigma_r}{\lambda}\right)^2 \qquad M\sigma_a^2 = \frac{1}{2T}\frac{\sigma_r^2}{\sigma_{\mathrm{Bd}}^2} \sim \frac{7}{T\ [\text{in weeks}]} \tag{7.2}$$

which are consistent with (3.2), (6.4), and (5.5). As mentioned, M is the decorrelation time constant measured in terms of revisit times. Keeping $\mathrm{SNR} = 1.5$ and $N = 30$ in Fig. 10, the dispersion shows the estimate of the subsidence rate in millimeters per year as a function of the frequency for different values (500, 50, 10) of the number of looks L and for a total observation time of one year (30 images at 12 days). In Fig. 11, I show, in the very same conditions, the number of pixels L_{PS} that is equivalent to a PS for various carrier frequencies according to the model. The constant in the approximation in (5.24) is definitely very

high, but it captures the behavior of the broad minimum with the frequency. I see from these figures that $L = 100$, for instance, is close enough to ensure that, with 12 days repeat and 30 revisits, the average coherence is enough to enter the PS regime $(1/N^3)$, so that the atmospheric effect is prevailing, and there is no appreciable change with the carrier frequency. Indeed, higher carrier frequencies behave worse, but practically big changes are not to be expected until 8–10 GHz. On the very low frequency side, the increment of the dispersion is due to the limited SNR, also as expected. With longer observation times, there would be a shift of the optimum toward lower frequencies while keeping the variation of the dispersion of the estimate rather small. In terms of the area $A_{\rm PS}$ to be occupied by the distributed scatterers to look like a PS, indicating with δ the spatial resolution, we can use (5.23) to say that $A_{\rm PS}$ is approximately independent of the frequency, as what is lost with M is gained with σ_a, i.e.,

$$A_{\rm PS} = \frac{0.75}{\sigma_a^2}\frac{N^2}{M}\delta^2 = 1.5N^2\delta^2\frac{\sigma_{\rm Bd}^2 T}{\sigma_r^2} \sim 0.1N^2T\ [\text{in weeks}]\ \delta^2. \qquad (7.3)$$

Further, as we can expect the resolution to improve with the carrier frequency, we can expect this area to decrease.

VIII. Conclusion

An evaluation of the subsidence rate error budget has been carried out for DInSAR interferometry using the three-day revisit interval data of ERS-1 over Rome. The results of modeling temporal decorrelation with a Brownian motion depend upon the number N of successive images used and the revisit interval T in weeks. Assuming a short-term target coherence of 0.6 and averaging measures over $L = 100$ independent looks, the dispersion of the velocity estimate is lower than 4–4.5 mm/year. For a wide band of frequencies, including C-band, the number of looks needed to make distributed scatterers as accurate as a PS is approximately on the order of $0.1N^2T$ [in weeks].

Acknowledgment

The author would like to thank Dr. F. De Zan, Prof. A. M. Guarnieri, and Dr. S. Tebaldini for helpful discussions and numerous contributions. Dr. De Zan carried out the analyses of the three-day Rome data. The author would also like to thank the reviewers for their very patient work, which helped a lot in increasing the readability of this paper, correcting many mistakes, and improving my notation.

References

[1] R. Bamler and P. Hartl, "Synthetic aperture radar interferometry," *Inv. Probl.*, vol. 14, no. 4, pp. R1–R54, 1998.

[2] P. M. L. Drezet and S. Quegan, "Environmental effects on the interferometric repeat-pass coherence of forests," *IEEE Trans. Geosci. Remote Sens.*, vol. 44, no. 4, pp. 825–837, Apr. 2006.

[3] A. Ferretti, C. Prati, and F. Rocca, "Permanent scatterers in SAR interferometry," *IEEE Trans. Geosci. Remote Sens.*, vol. 39, no. 1, pp. 8–20, Jan. 2001.

[4] A. Ferretti, D. Perissin, C. Prati, and F. Rocca, "On the physical nature of SAR permanent scatterers," in *Proc. URSI Commission F Symp. Microw. Remote Sens. Earth, Oceans, Ice and Atmosphere*, Ispra, Italy, Apr. 20–21, 2005, p. 6.

[5] Y. Fialko, "Interseismic strain accumulation and the earthquake potential on the southern San Andreas fault system," *Nature*, vol. 441, no. 7096, pp. 968–971, Jun. 2006.

[6] G. Franceschetti and G. Fornaro, "Synthetic aperture radar interferometry," in *Synthetic Aperture Radar Processing*, G. Franceschetti and R. Lanari, Eds. Boca Raton, FL: CRC Press, 1999, ch. 4, pp. 167–223.

[7] A. K Gabriel, R. M Goldstein, and H. A Zebker, "Mapping small elevation changes over large areas: Differential radar interferometry," *J. Geophys. Res.*, vol. 94, no. B7, pp. 9183–9191, Jul. 10, 1989.

[8] F. Gatelli, A. Monti Guarnieri, F. Parizzi, P. Pasquali, C. Prati, and F. Rocca, "The wavenumber shift in SAR interferometry," *IEEE Trans. Geosci. Remote Sens.*, vol. 32, no. 4, pp. 855–865, Jul. 1994.

[9] R. M. Goldstein and H. A. Zebker, "Interferometric radar measurement of ocean surface currents," *Nature*, vol. 328, no. 20, pp. 707–709, Aug. 1987.

[10] R. F. Hanssen, *Radar Interferometry: Data Interpretation and Error Analysis*. Dordrecht, The Netherlands: Kluwer, 2001.

[11] R. F. Hanssen, "Satellite radar interferometry for deformation monitoring: A priori assessment of feasibility and accuracy," *Int. J. Appl. Earth Observation and Geoinformation*, vol. 6, no. 3/4, pp. 253–260, Mar. 2005.

[12] A. Hooper, H. Zebker, P. Segall, and B. Kampes, "A new method for measuring deformation on volcanoes and other natural terrains using InSAR persistent scatterers," *Geophys. Res. Lett.*, vol. 31, no. 23, L23611, 2004. DOI:10.1029/2004GL021737.

[13] O. Ledoit and M. Wolf, "Honey, I shrunk the sample covariance matrix," *J. Portf. Manage.*, vol. 31, no. 1, Fall 2004.

[14] F. Rocca, C. Prati, P. Pasquali, and A. Monti Guarnieri, "SAR interferometry techniques and applications," ESA, Noordwijk, The Netherlands, Tech. Rep. 7439/92/HGE-I, 1994.

[15] F. Rocca, "Diameters of the orbital tubes in long-term interferometric SAR surveys," *IEEE Geosci. Remote Sens. Lett.*, vol. 1, no. 3, pp. 224–227, Jul. 2004.

[16] P. Rosen, S. Hensley, I. R. Joughin, F. K. Li, S. Madsen, E. Rodríguez, and R. Goldstein, "Synthetic aperture radar interferometry," *Proc. IEEE*, vol. 88, no. 3, pp. 333–382, Mar. 2000.

[17] Sentinel-1 MRD. [Online]. Available: http://esamultimedia.esa.int/docs/GMES/GMES_SENT1_MRD_1-4_approved_version.pdf

[18] S. Tebaldini and A. Monti Guarnieri, "Cramér–Rao lower bound for parametric phase estimation in multi-pass radar interferometry," *Analysis of Ambiguity Noise in the Sentinel-1 Interferometric Wideswath Mode*. Personal Communication, Final report, ESA Contract 19142/05/NL/CB.

[19] R. Touzi, A. Lopes, J. Bruniquel, and P. W. Vachon"Coherence estimation for SAR imagery," *IEEE Trans. Geosci. Remote Sens.*, vol. 37, no. 1, pp. 135–149, Jan. 1999.

[20] H. Van Trees, *Optimum Array Processing*. New York: Wiley-Interscience, 2002.

[21] H. A. Zebker and J. Villasenor, "Decorrelation in interferometric radar echoes," *IEEE Trans. Geosci. Remote Sens.*, vol. 30, no. 5, pp. 950–959, Sep. 1992.

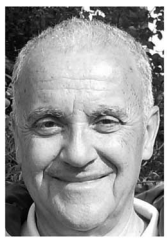

Fabio Rocca received the Dottore degree in ingegneria elettronica from Politecnico di Milano, Milano, Italy, in 1962.

He is currently a Professor of digital signal processing with the Dipartimento di Elettronica ed Informazione, Politecnico di Milano, Milano, Italy. He made research on digital signal processing for television bandwidth compression, emission tomography, seismic data processing, and SAR. During 1978–1988, he was a Visiting Professor at Stanford University, Stanford, CA. He was a Department Chair of the Istituto di Elettrotecnica ed Elettronica of the Politecnico di Milano during 1975–1978, a Cofounder of two small technological spin-off companies from Politecnico di Milano, namely Telerilevamento Europa and Aresys, a past President of the European Association of Exploration Geophysicists (EAEG), an Honorary Member of Society of Exploration Geophysicists (SEG) in 1989 and European Association of Geoscientists and Engineers (EAGE) in 1998, the President of the Istituto Nazionale di Oceanografia e di Geofisica Sperimentale (OGS) Trieste during 1982–1983, a member of the Scientific Council of OGS, and a member of the SAR Advisory Group of the European Space Agency.

Dr. Rocca received an award from Italgas Telecommunications in 1995, a Special SEG Commendation in 1998, the Eduard Rhein Foundation Technology Award in 1999, and the Doctorat Honoris Causa in Geophysics, Institut National Polytechnique de Lorraine, Nancy, France, in 2001. He also received best paper awards at the International Geoscience and Remote Sensing Symposium in 1989 and 1999 and at the European Conference on Synthetic Aperture Radar in 2004.